nature physics

ARTICLES

PUBLISHED ONLINE: 3 NOVEMBER 2013 | DOI: 10.1038/NPHYS2790

Direct measurement of the Zak phase in topological Bloch bands

Marcos Atala[1†], Monika Aidelsburger[1†], Julio T. Barreiro[1,2], Dmitry Abanin[3], Takuya Kitagawa[3,4], Eugene Demler[3] and Immanuel Bloch[1,2*]

Geometric phases that characterize the topological properties of Bloch bands play a fundamental role in the band theory of solids. Here we report on the measurement of the geometric phase acquired by cold atoms moving in one-dimensional optical lattices. Using a combination of Bloch oscillations and Ramsey interferometry, we extract the Zak phase—the Berry phase gained during the adiabatic motion of a particle across the Brillouin zone—which can be viewed as an invariant characterizing the topological properties of the band. For a dimerized lattice, which models polyacetylene, we measure a difference of the Zak phase $\delta\varphi_{\mathrm{Zak}} = 0.97(2)\pi$ for the two possible polyacetylene phases with different dimerization. The two dimerized phases therefore belong to different topological classes, such that for a filled band, domain walls have fractional quantum numbers. Our work establishes a new general approach for probing the topological structure of Bloch bands in optical lattices.

The non-trivial topological structure of Bloch bands in solids gives rise to fundamental physical phenomena, including fermion number fractionalization[1–4], the integer quantum Hall effect[5,6], as well as topologically protected surface states in topological insulators[7,8]. The topological character of a Bloch band is defined by certain invariants, which can be expressed in terms of the Berry's phase[9] acquired by a particle during adiabatic motion through the band[6,8]. The most well-known example is the two-dimensional (2D) topological invariant, the first Chern number, which is related to the Berry's phase for a contour enclosing the Brillouin zone and determines the quantized value of the Hall conductivity of a filled 2D band[5,6]. For 1D systems, topological invariants of Bloch bands have been discussed theoretically[6,8,10–12]; however, they have never been measured in any experiment.

Here we present direct measurements of Berry's phase and topological invariants of 1D periodic potentials using systems of ultracold atoms in optical lattices. The topological properties of 1D solids are characterized by the so-called Zak phase—the Berry's phase picked up by a particle moving across the Brillouin zone[12]. For a given Bloch wave $\psi_k(x)$ with quasimomentum k, the Zak phase, φ_{Zak}, can be conveniently expressed through the cell-periodic Bloch function $u_k(x) = \mathrm{e}^{-ikx}\psi_k(x)$:

$$\varphi_{\mathrm{Zak}} = i\int_{-G/2}^{G/2} \langle u_k|\partial_k|u_k\rangle \,\mathrm{d}k \qquad (1)$$

where $G = 2\pi/d$ is the reciprocal lattice vector, d is the lattice period and ∂_k is the partial derivative with respect to k (ref. 12). Non-trivial Zak phases underlie the existence of protected edge states[13,14], fermion number fractionalization[1–3], and irrationally charged domain walls[15,16] between topologically distinct 1D solids. These phenomena, initially discussed in the context of quantum field theory[1,2,15], subsequently found condensed matter realizations in polyacetylene[3], described by the celebrated Su-Schrieffer-Heeger (SSH) model, and linearly conjugated diatomic polymers[16].

In our experiment, the key idea is to combine coherent Bloch oscillations with Ramsey interferometry to determine the geometric Zak phase and reveal the underlying topological character of the Bloch bands. Previously, the measurement of topological invariants was confined to 2D bands by exploiting the relationship between the Chern number and the Hall conductivity for a filled band given by the Thouless–Kohmoto–Nightingale–DeNijs (TKNN) equations[5]. There the integration over the Brillouin zone necessary to determine the topological invariant was achieved through filling of the underlying Bloch band. In contrast, in our case the integration over the Brillouin zone necessary for extracting topological invariants is achieved by adiabatic transport of a single-particle wave packet through the band using Bloch oscillations. Recently, it has also been suggested that in the context of ultracold atoms, topological properties could be studied through time-of-flight images[17–19] or measurements of anomalous velocity[6,20].

In the following we focus on a dimerized optical lattice with two sites per unit cell—a system which, despite its simplicity, exhibits rich topological physics, and depending on the parameter values can mimic either polyacetylene[3] or conjugated diatomic polymers[16]. Within a tight-binding model, the physics of such a system is captured by the Rice–Mele Hamiltonian[16]:

$$\begin{aligned}\hat{H} = &-\sum_n \left(J\hat{a}_n^\dagger\hat{b}_n + J'\hat{a}_n^\dagger\hat{b}_{n-1} + \mathrm{h.c.}\right)\\ &+ \Delta\sum_n (\hat{a}_n^\dagger\hat{a}_n - \hat{b}_n^\dagger\hat{b}_n)\end{aligned} \qquad (2)$$

where J, J' denote modulated tunnelling amplitudes within the unit cell, $\hat{a}_n^\dagger(\hat{b}_n^\dagger)$ are the particle creation operators for an atom

[1]Fakultät für Physik, Ludwig-Maximilians-Universität, Schellingstraße 4, 80799 Munich, Germany, [2]Max-Planck Institute of Quantum Optics, Hans-Kopfermann Straße 1, 85748 Garching, Germany, [3]Department of Physics, Harvard University, 17 Oxford Street, Cambridge, Massachusetts 02138, USA, [4]Rakuten.Inc, Shinagawa Seaside Rakuten Tower, 4-12-3, 140-0002 Tokyo, Japan. †These authors contributed equally to this work.
*e-mail: immanuel.bloch@mpq.mpg.de

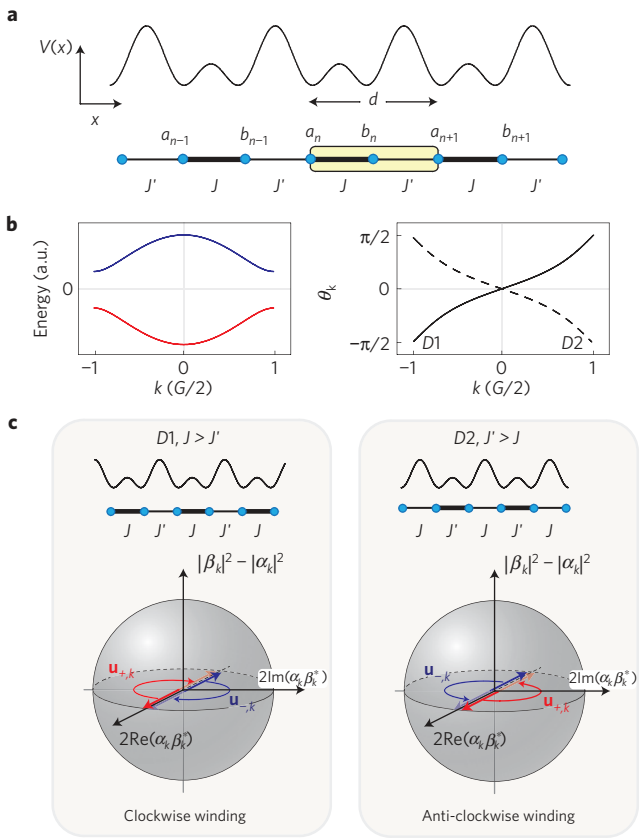

Figure 1 | Energy bands and topology of dimerized lattice model. **a**, Schematic illustration of the optical superlattice potential used in the experiment to realize the SSH model (yellow box denotes the unit cell of size $d = \lambda_s$). **b**, Exemplary curves for the lower and upper energy bands (red and blue lines) and phase θ_k for dimerization $D1$ and $D2$ (solid and dashed line) as a function of quasimomentum k. **c**, Pseudo-spin representation of the eigenstates $\mathbf{u}_{\mp,k}$ of the upper and lower energy bands for the two dimerization configurations $D1$ and $D2$. The pseudo-spin vectors $\mathbf{u}_{\mp,k}$ point in opposite directions and exhibit the same sense of rotation (winding) with quasimomentum k. In the phase $D1$ ($D2$) $\mathbf{u}_{\mp,k}$ evolve (anti-) clockwise and therefore exhibit opposite winding.

on the sublattice site $a_n(b_n)$ in the nth lattice cell (Fig. 1a), and Δ characterizes the energy offset between neighbouring lattice sites.

When the on-site energies of the two sites are tuned to be equal ($\Delta = 0$), our system corresponds to the SSH model of polyacetylene (Fig. 1a). In this case, $\hat{H}$ is known to exhibit two topologically distinct phases, $D1$ for $J > J'$, and $D2$ for $J < J'$, separated by a topological phase transition point at $J = J'$. The distinct topological character of the two phases is reflected in the difference of their Zak phases, for which $\delta\varphi_{\mathrm{Zak}} = \pi$. When the on-site energies are tuned to be different ($\Delta \neq 0$), our system models a linearly conjugated diatomic polymer; in this case, the difference of the Zak phases is fractional in units of π.

In the experiment, we realized the Hamiltonian $\hat{H}$ of equation (2) by loading a Bose–Einstein condensate of ^{87}Rb into a 1D optical superlattice potential[21]. This potential was formed by superimposing two standing optical waves of wavelengths $\lambda_s = 767$ nm and $\lambda_l = 2\lambda_s = 1{,}534$ nm that generate a lattice potential of the form $V(x) = V_l \sin^2(k_l x + \phi/2) + V_s \sin^2(2k_l x + \pi/2)$, where $k_l = 2\pi/\lambda_l$ and V_s and V_l are the corresponding strengths of the two standing waves (Fig. 1a). Phase control between the two standing wave fields enabled us to fully control ϕ. For example, switching between $\phi = 0$ and $\phi = \pi$ allowed us to rapidly access the two different dimerized configurations $D1$ ($D2$) with $\Delta = 0$ in the experiment, whereas by tuning ϕ slightly away from these symmetry points we could introduce a controlled energy offset Δ.

The eigenstates of $\hat{H}$ can be written as Bloch waves of the form:

$$\psi_k(x) = \mathrm{e}^{ikx} u_k(x) = \sum_n \alpha_k \mathrm{e}^{ikx_n} w_a(x - x_n) + \beta_k \mathrm{e}^{ik(x_n + d/2)} w_b(x - x_n - d/2)$$

where $x_n = nd$ with n integer, and $w_{a,b}(x)$ are the Wannier functions[22] for a_n, b_n sites, respectively. The coefficients α_k, β_k are determined through the eigenvalue equation $\hat{H}\psi_k = E_k\psi_k$. In this case, the cell-periodic wavefunction u_k can be viewed as a two-component spinor $\mathbf{u}_k = (\alpha_k, \beta_k)$, and equation (1) for the Zak phase takes an especially simple form:

$$\varphi_{\mathrm{Zak}} = i\int_{-G/2}^{G/2} \left(\alpha_k^* \partial_k \alpha_k + \beta_k^* \partial_k \beta_k\right) \mathrm{d}k$$

For our choice of the unit cell (Supplementary Information), the eigenfunctions for the lower (upper) band of the SSH model ($\Delta = 0$) are

$$\mathbf{u}_{\mp,k} = \frac{1}{\sqrt{2}} \begin{pmatrix} \pm 1 \\ \mathrm{e}^{-i\theta_k} \end{pmatrix}$$

where θ_k is determined through $J\mathrm{e}^{ikd/2} + J'\mathrm{e}^{-ikd/2} = |\epsilon_k|\mathrm{e}^{i\theta_k}$ (Supplementary Information). We can thus visualize the Bloch periodic functions as pseudo spin-1/2 states oriented in the equatorial plane of a Bloch sphere (Fig. 1c). Note also that although $\psi_{k+G}(x) = \psi_k(x)$, this translational invariance is not true for $\mathbf{u}_{\mp,k}$, because in our system with a two-site unit cell $\mathbf{u}_{\mp,k+G} = \hat{\sigma}_z \mathbf{u}_{\mp,k}$, where $\hat{\sigma}_z$ is the third Pauli matrix. As the two state vectors for the upper and lower bands are orthogonal, they point in opposite directions and therefore exhibit the same winding when the quasimomentum k is varied adiabatically. The Zak phases for the lower and upper band are thus identical $\varphi_{\mathrm{Zak}}^{D1} = \pi/2$. However, when the dimerization is changed from configuration $D1$ to $D2$ (Fig. 1c), the corresponding geometric phase changes to $\varphi_{\mathrm{Zak}}^{D2} = -\pi/2$, because of the opposite winding of the state with quasimomentum k. The difference between the two Zak phases for the two dimerized configurations is then:

$$\delta\varphi_{\mathrm{Zak}} = \varphi_{\mathrm{Zak}}^{D1} - \varphi_{\mathrm{Zak}}^{D2} = \pi \qquad (3)$$

We must point out that the Zak phase of each dimerization is a gauge dependent quantity—that is, it depends on the choice of origin of the unit cell; however, the difference between the Zak phases of the two dimerizations is uniquely defined[8,23]. There is, however, a natural choice of the origin of the unit cell with which one can identify which dimerization configuration is topologically trivial or non-trivial (Supplementary Section X).

When an atom is adiabatically evolved through the Brillouin zone of the periodic potential $k \to k + G$, it acquires a phase shift due to three distinct contributions: a geometric phase φ_{Zak} as well as a dynamical phase $\varphi_{\mathrm{dyn}} = \int E(t)/\hbar\,\mathrm{d}t$, both derived from the band-structure, and a phase due to the Zeeman energy of the atom in an external magnetic field (see semiclassical analysis in the Supplementary Information):

$$\varphi_{\mathrm{tot}} = \varphi_{\mathrm{Zak}} + \varphi_{\mathrm{dyn}} + \varphi_{\mathrm{Zeeman}}$$

To isolate the geometric Zak phase in the experiment, we employ a three-step sequence (Fig. 2a and Supplementary Information). Step (1) We start with an atom in the state $|{\downarrow}, k = 0\rangle$ and bring it into a coherent superposition state $1/\sqrt{2}(|{\uparrow}, k = 0\rangle + |{\downarrow}, k = 0\rangle)$ using a microwave $\pi/2$-pulse. Here $\sigma = \uparrow, \downarrow$ denotes two spin states of the atom with opposite magnetic moment. Then a magnetic

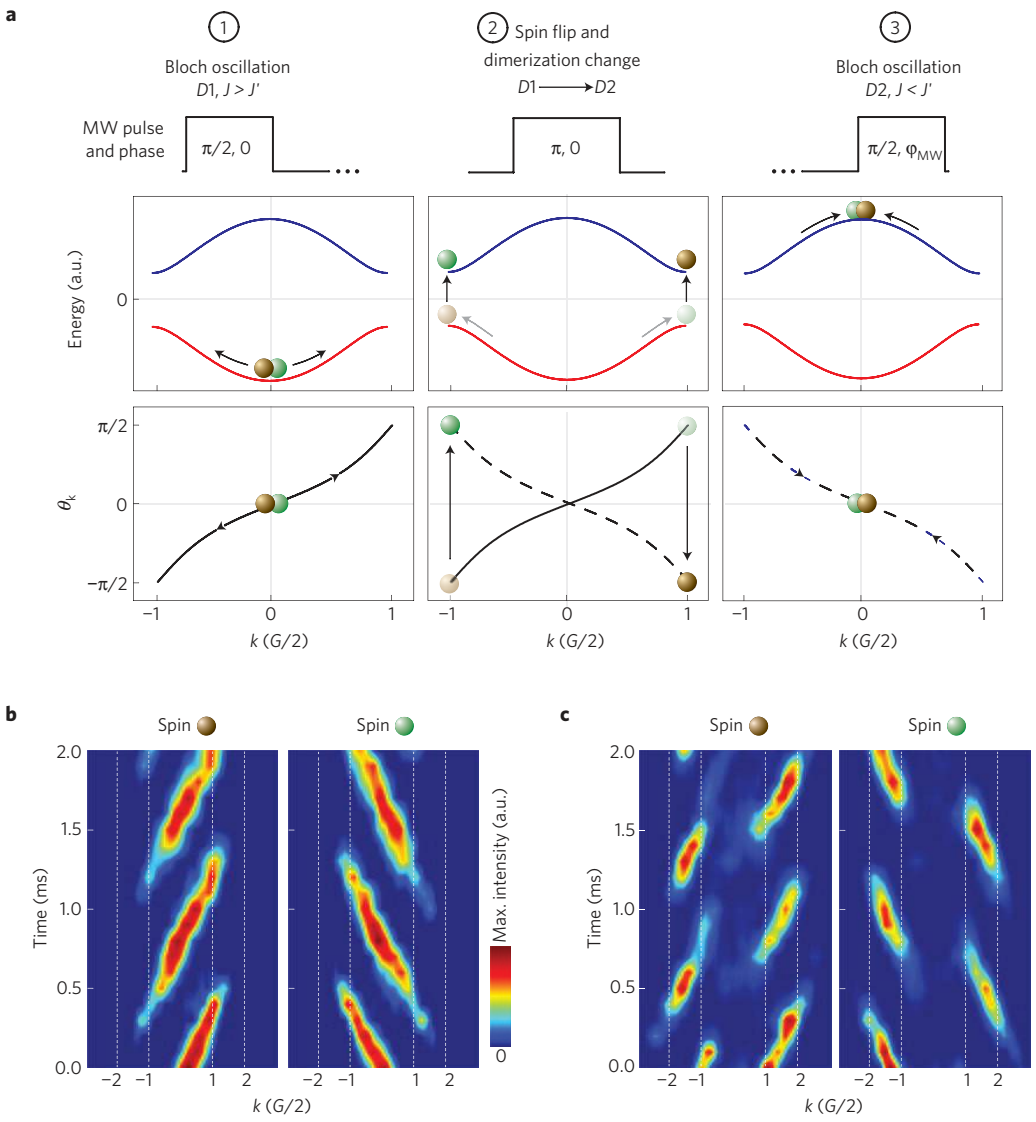

Figure 2 | Experimental sequence and spin-dependent Bloch oscillations. a, Energy band, MW pulses and state evolution of a single atom in a superposition of two spin-states with opposite magnetic moment (brown and green balls) during the three-step echo sequence described in the text. The winding of the state vector with k is given by θ_k (solid line dimerization $D1$, dashed line dimerization $D2$). **b**,**c**, Time-of-flight momentum distributions taken for different evolution times of the spin-dependent Bloch oscillations in the lower (**b**) and upper energy band (**c**) used in the experiment. Each momentum point is an average of three identical measurements.

field gradient is applied that creates a constant force in opposite directions for the two spin components. Such a constant force leads to Bloch oscillations—that is, a linear evolution of quasimomentum over time[24]. In our case the force is directed in opposite directions for the two spin components. The atomic wavepacket thus evolves into the coherent superposition state $1/\sqrt{2}(|\uparrow,k\rangle + e^{i\delta\varphi}|\downarrow,-k\rangle)$. When both reach the band edge, the differential phase between the two states is given by $\delta\varphi = \varphi_{\mathrm{Zak}} + \delta\varphi_{\mathrm{Zeeman}}$. Note that for all time-reversal invariant Hamiltonians (as is the case here), the dynamical phase acquired during the adiabatic evolution is equal for the two spin states and therefore cancels in the phase difference. In principle, if a sufficiently high magnetic field stability is present in the laboratory such that $\varphi_{\mathrm{Zeeman}}$ is reproducible, one could end the experimental sequence here by applying a second $\pi/2$-pulse with phase φ_{MW}, as described in step 3 below. The Zak phase of the lowest band could then be directly extracted from the resulting Ramsey fringe. Step (2) To eliminate the Zeeman phase difference, we apply a spin-echo π-pulse at this point and also switch dimerization from $D1 \rightarrow D2$. For atoms located at the band edge $k = \pm G/2$, this non-adiabatic dimerization switch induces a transition to the excited band of the SSH model. Step (3) The sequence is finally completed by letting the spin components further evolve in the upper band until they return to $k = 0$. At this point in time, a final $\pi/2$-pulse with phase φ_{MW} is applied to interfere the two spin components and read out their relative phase $\delta\varphi$ through the resulting Ramsey fringe. The change in dimerization occurring at the mid-point of the echo sequence is crucial in order not to cancel the Zak phase in addition to the Zeeman phase. As a result of the opposite windings of the Bloch states in the upper and lower bands with quasimomentum k (Fig. 1c), the resulting phase shift encoded in the Ramsey fringe is thus given by $\delta\varphi = \varphi_{\mathrm{Zak}}^{D1} - \varphi_{\mathrm{Zak}}^{D2}$ if the dimerization is swapped, whereas $\delta\varphi = 0$ if it is left unchanged.

In Fig. 2b,c we show images of the momentum distribution of the atoms during the spin-dependent Bloch oscillations in the lower and upper energy bands. Note the opposite evolution in momentum space due to the opposite magnetic moments of the

two spin-states. Atoms in the upper energy band are characterized by a distinctively different momentum pattern from atoms in the lower energy band. The period of the Bloch oscillations, $\tau_{\mathrm{Bloch}} = 0.85(3)$ ms, was chosen to be slow enough, such that non-adiabatic Landau–Zener transitions at the band edge are negligible, while still maintaining an overall fast evolution time to minimize decoherence effects.

A typical result for the two Ramsey fringes obtained with and without dimerization swapping during the state evolution can be seen in Fig. 3a. Each plotted value for a given angle φ_{MW} is an average over five identical measurements to reduce the effect of residual fluctuations. We performed a further statistical analysis by recording 14 independent Ramsey fringes for the two configurations. The obtained phase differences are shown in Fig. 3b, together with the corresponding histogram. From these individual measurements we determine the geometric phase difference between the two dimerized configurations to be:

$$\delta\varphi = 0.97(2)\pi$$

in excellent agreement with theory, as discussed above (see equation (3)). The uncertainty in the recorded value denotes the standard error of the mean obtained from the distribution function (Fig. 3b) and is mainly determined by experimental imperfections in the control of the underlying lattice potentials, particularly of the relative phase ϕ between the two standing waves.

To further demonstrate the generality of our method, we studied the dependence of the Zak phase on a staggered on-site energy Δ (Fig. 4a and equation (2)). This corresponds to a heteropolar dimer configuration[16], where the value of the Zak phase is non-quantized. The energy offset Δ displaces the pseudo-spin Bloch vectors away from the equatorial plane:

$$\mathbf{u}_{-,k} = \begin{pmatrix} \sin\frac{\gamma_k}{2} \\ \cos\frac{\gamma_k}{2}\mathrm{e}^{-i\theta_k} \end{pmatrix},$$

$$\mathbf{u}_{+,k} = \begin{pmatrix} -\cos\frac{\gamma_k}{2} \\ \sin\frac{\gamma_k}{2}\mathrm{e}^{-i\theta_k} \end{pmatrix},$$

$$\gamma_k = \arctan\frac{\epsilon_k}{\Delta}$$

resulting in a further dependence of the Zak phase on the offset Δ and the band index (Fig. 4a and Supplementary Information).

To probe the dependence of φ_{Zak} on Δ, we performed an experimental sequence that was similar to the one described above. However, instead of swapping the dimerization from $D1$ to $D2$, an energy offset $|\Delta| < 2J$ was introduced for one half of the sequence. Thereafter, because of the spin-echo pulse, the wavepackets return to $k = 0$ in the lowest band. Although the system completes a full Bloch oscillation in the lowest band, the total geometric phase acquired is not zero, because the Bloch vector is displaced from the equatorial plane during one half of the sequence (Fig. 4) and the Zak phase is changed from φ_{Zak} to $\varphi_{\mathrm{Zak}}(\Delta)$. The resulting phase in the Ramsey fringe is thus given by $\delta\varphi = \varphi_{\mathrm{Zak}} - \varphi_{\mathrm{Zak}}(\Delta)$ when the energy offset is present, and $\delta\varphi = 0$ when the offset is absent. As before, the phase difference between these two fringes for atoms in the lowest band allows us to determine the relative phase $\varphi_{\mathrm{Zak}} - \varphi_{\mathrm{Zak}}(\Delta)$. During the non-adiabatic switching of the superlattice potential at step 2 of the experimental sequence, some of the atoms are transferred to the higher band and acquire a different geometric phase. However, taking into account this contribution to the measured phase difference enabled us to extract the relative phase $\delta\varphi$ from our data (Supplementary Information). As shown in Fig. 4b, we find good agreement between the measured and predicted values of the fractional Zak phase. Fractional Zak

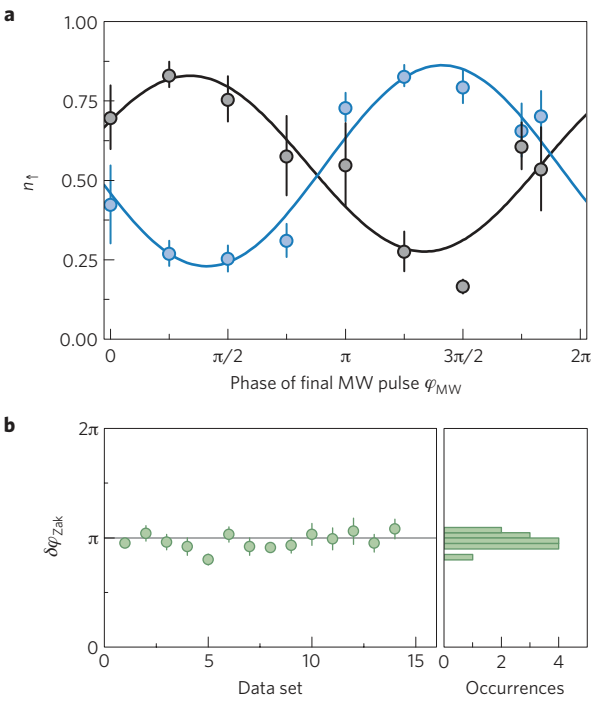

Figure 3 | Determination of the Zak phase. a, Following the sequence described in the text, the atom number in the two spin states, $N_{\uparrow,\downarrow}$, is measured and the fraction of atoms in the $|\uparrow\rangle$ spin state, $n_\uparrow = N_\uparrow/(N_\uparrow + N_\downarrow)$, is plotted as a function of the phase of the final microwave $\pi/2$-pulse. Blue (black) circles correspond to the fringe in which the dimerization was (not) swapped, and the corresponding solid lines are sinusoidal fits to the data, where the free parameters were the amplitude, offset and initial phase. The difference in phase of the two fits to the Ramsey fringes yields the Zak phase difference $\delta\varphi_{\mathrm{Zak}} = \varphi^{D1}_{\mathrm{Zak}} - \varphi^{D2}_{\mathrm{Zak}}$. To reduce the effect of fluctuations, every data point is an average of five individual measurements and the error bars show the standard deviation of the mean. The phase of the reference fringe (black) is determined by a small detuning of the microwave pulse (Supplementary Information). **b**, Measured relative phase for 14 identical experimental runs (left), which give an average value of $\delta\varphi_{\mathrm{Zak}} = 0.97(2)\pi$. The corresponding histogram is shown on the right with a binning of 0.05π. The 1σ-width of the resulting distribution is $\sigma = 0.07\pi$.

phases could also be determined by carrying out one full Bloch oscillation cycle for each of the spin states. The dynamical phase would then be cancelled even for general lattice structures without time-reversal symmetry and the resulting Ramsey phase would correspond to $2\varphi_{\mathrm{Zak}}$.

In conclusion, we have presented a general approach for studying the topological properties of Bloch bands in optical lattices and demonstrated its versatility through a first measurement of the topological invariant in topologically non-trivial Bloch bands. Topologically distinct many-body phases can arise from such topologically distinct Bloch bands when the bands are filled with fermions. Making use of the recently demonstrated control of optical potentials at the single-site level[25], we plan to realize domain walls or sharp boundaries in the dimerized lattice that would allow us to directly study edge states[26,27] and fractional charges for non-interacting fermions or hardcore bosons[1–3,28,29]. Although in this work we focused on 1D systems, our technique can easily be extended to 2D systems, where the change of the Zak phase in the Brillouin zone gives the topological density of the Bloch band[30]. This enables measurements of both the Chern number of topological bands and the π-flux associated with a Dirac point. Additionally, we expect that this idea can be extended to measure

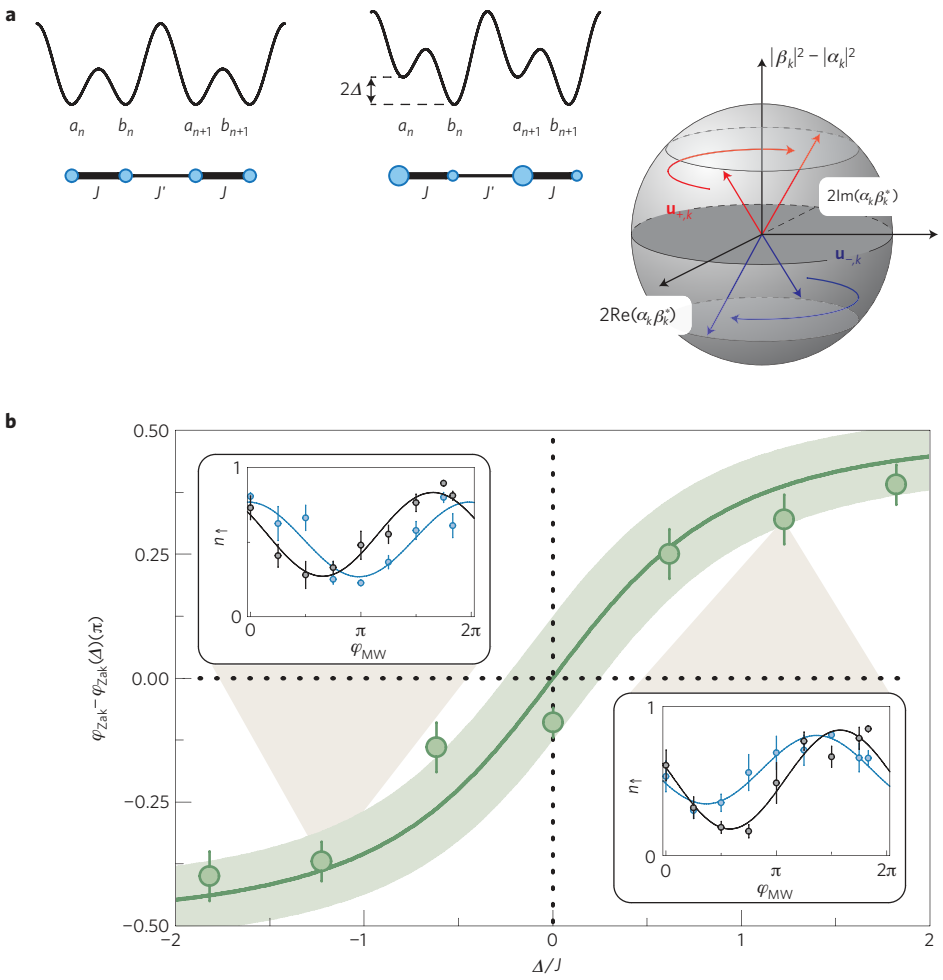

Figure 4 | Fractional Zak phase. a, Lattice potential without and with an on-site energy staggering Δ. When $\Delta = 0$ the Zak phase is $\varphi_{Zak}(\Delta = 0) = \pi/2$. As Δ increases, the pseudo-spin vectors of the lower (blue vector) and upper (red vector) band move away from the equatorial plane and the value of $\varphi_{Zak}(\Delta)$ decays rapidly to zero. **b**, Measured phase difference $\varphi_{Zak} - \varphi_{Zak}(\Delta)$ as a function of Δ. Each individual point was obtained from four individual measurements. The vertical error bars represent the standard error of the mean. The green line is the theoretical prediction and the shaded area represents the uncertainties in the calibration of the energy offset Δ. The insets show a typical Ramsey fringe for $\Delta/J = -1.2$ (left) and $\Delta/J = 1.2$ (right), which were used to extract the relative phase $\delta\varphi$. The blue (black) fringes correspond to measurements with (without) staggering (Supplementary Information).

the non-Abelian Berry's phase in Bloch bands, such as in a system with the quantum spin Hall effect[31], to the study of Floquet states in periodically driven systems[32–34], and to quasiparticles in unconventional superconductors, such as d-wave superconductors, which have Dirac dispersions at the nodal points[35]. Overall, our work indicates that cold atomic systems provide a versatile platform for studying topological states of matter, and establishes a novel method for probing their properties.

Received 11 June 2013; accepted 27 September 2013; published online 3 November 2013

References

1. Jackiw, R. & Rebbi, C. Solitons with fermion number 1/2. *Phys. Rev. D* **13,** 3398–3409 (1976).
2. Goldstone, J. & Wilczek, F. Fractional quantum numbers on solitons. *Phys. Rev. Lett.* **47,** 986–989 (1981).
3. Su, W. P., Schrieffer, J. R. & Heeger, A. J. Solitons in polyacetylene. *Phys. Rev. Lett.* **42,** 1698–1701 (1979).
4. Bell, J. S. & Rajaraman, R. On states, on a lattice, with half-integer charge. *Nucl. Phys. B* **220,** 1–12 (1983).
5. Thouless, D. J., Kohmoto, M., Nightingale, M. P. & den Nijs, M. Quantized Hall conductance in a two-dimensional periodic potential. *Phys. Rev. Lett.* **49,** 405–408 (1982).
6. Xiao, D., Chang, M-C. & Niu, Q. Berry phase effects on electronic properties. *Rev. Mod. Phys.* **82,** 1959–2007 (2010).
7. Hasan, M. Z. & Kane, C. L. Colloquium: Topological insulators. *Rev. Mod. Phys.* **82,** 3045–3067 (2010).
8. Qi, X. & Zhang, S. Topological insulators and superconductors. *Rev. Mod. Phys.* **83,** 1057–1110 (2011).
9. Berry, M. V. Quantal phase factors accompanying adiabatic changes. *Proc. R. Soc. Lond. A* **392,** 45–57 (1984).
10. Kitaev, A. Periodic table for topological insulators and superconductors. *AIP Conf. Proc.* **1134,** 22–30 (2009).
11. Ryu, S., Schneider, A., Furusaki, A. & Ludwig, A. Topological insulators and superconductors: tenfold way and dimensional hierarchy. *New J. Phys.* **12,** 065010 (2010).
12. Zak, J. Berry's phase for energy bands in solids. *Phys. Rev. Lett.* **62,** 2747–2750 (1989).
13. Ryu, S. & Hatsugai, Y. Topological origin of zero-energy edge states in particle–hole symmetric systems. *Phys. Rev. Lett.* **89,** 077002 (2002).
14. Delplace, P., Ullmo, D. & Montambaux, G. Zak phase and the existence of edge states in graphene. *Phys. Rev. B* **84,** 195452 (2011).
15. Niemi, A. J. & Semenoff, G. W. Spectral asymmetry on an open space. *Phys. Rev. D* **30,** 809–818 (1984).
16. Rice, M. J. & Mele, E. J. Elementary excitations of a linearly conjugated diatomic polymer. *Phys. Rev. Lett.* **49,** 1455–1459 (1982).
17. Alba, E. *et al.* Seeing topological order in time-of-flight measurements. *Phys. Rev. Lett.* **107,** 235301 (2011).
18. Zhao, E. *et al.* Chern numbers hiding in time-of-flight images. *Phys. Rev. A* **84,** 063629 (2011).

19. Goldman, N. *et al.* Measuring topology in a laser-coupled honeycomb lattice: From Chern insulators to topological semi-metals. *New J. Phys.* **15,** 013025 (2013).
20. Price, H. M. & Cooper, N. R. Mapping the Berry curvature from semiclassical dynamics in optical lattices. *Phys. Rev. A* **85,** 033620 (2012).
21. Fölling, S. *et al.* Direct observation of second-order atom tunnelling. *Nature* **448,** 1029–1032 (2007).
22. Wannier, G. H. Dynamics of band electrons in electric and magnetic fields. *Rev. Mod. Phys.* **34,** 645–655 (1962).
23. King-Smith, R. D. & Vanderbilt, D. Theory of polarization of crystalline solids. *Phys. Rev. B* **47,** 1651–1654 (1993).
24. Ben Dahan, M., Peik, E., Reichel, J., Castin, Y. & Salomon, C. Bloch oscillations of atoms in an optical potential. *Phys. Rev. Lett.* **76,** 4508–4511 (1996).
25. Weitenberg, C. *et al.* Single-spin addressing in an atomic Mott insulator. *Nature* **471,** 319–324 (2011).
26. Kitagawa, T. *et al.* Observation of topologically protected bound states in photonic quantum walks. *Nature Commun.* **3,** 882 (2012).
27. Kraus, Y. E. *et al.* Topological states and adiabatic pumping in quasicrystals. *Phys. Rev. Lett.* **109,** 106402 (2012).
28. Ruostekoski, J., Dunne, G. & Javanainen, J. Particle number fractionalization of an atomic Fermi–Dirac gas in an optical lattice. *Phys. Rev. Lett.* **88,** 180401 (2002).
29. Grusdt, F., Hoening, M. & Fleischhauer, M. Topological edge states in the one-dimensional super-lattice Bose–Hubbard model. *Phys. Rev. Lett.* **110,** 260405 (2013).
30. Abanin, D. *et al.* Interferometric approach to measuring band topology in 2D optical lattices. *Phys. Rev. Lett.* **110,** 165304 (2013).
31. Kane, C. L. & Mele, E. J. Quantum spin Hall effect in graphene. *Phys. Rev. Lett.* **95,** 226801 (2005).
32. Grifoni, M. & Hänggi, P. Driven quantum tunneling. *Phys. Rep.* **304,** 229–354 (1998).
33. Kitagawa, T., Berg, E., Rudner, M. & Demler, E. Topological characterization of periodically driven quantum systems. *Phys. Rev. B* **82,** 235114 (2010).
34. Lindner, N. H., Refael, G. & Galitski, V. Floquet topological insulator in semiconductor quantum wells. *Nature Phys.* **7,** 490–495 (2011).
35. Volovik, G. E. *The Universe in a Helium Droplet* (Oxford Univ. Press, 2003).

Acknowledgements

We acknowledge helpful discussions with B. Paredes. We thank Y-A. Chen and S. Nascimbène for their help in setting up the experiment and for their comments in the early stages of the experiment. This work was supported by the DFG (FOR635, FOR801), NIM, DARPA (OLE program), Harvard-MIT CUA, the ARO-MURI on Atomtronics, and the ARO MURI Quism program. M. Aidelsburger was further supported by the Deutsche Telekom Stiftung.

Author contributions

M. Atala, M. Aidelsburger and J.T.B. carried out the experiments and the data analysis. D.A., T.K. and E.D. carried out the theoretical analysis and derived the measurement protocol. I.B. and E.D. supervised the work and developed the general measurement idea. All authors contributed extensively to the analysis and the writing of the manuscript.

Additional information

Supplementary information is available in the online version of the paper. Reprints and permissions information is available online at www.nature.com/reprints. Correspondence and requests for materials should be addressed to I.B.

Competing financial interests

The authors declare no competing financial interests.